

The El Salvador and Philippines Tsunamis of August 2012: Insights from Sea Level Data Analysis and Numerical Modeling

MOHAMMAD HEIDARZADEH^{1,2} and KENJI SATAKE¹

Abstract—We studied two tsunamis from 2012, one generated by the El Salvador earthquake of 27 August (M_w 7.3) and the other generated by the Philippines earthquake of 31 August (M_w 7.6), using sea level data analysis and numerical modeling. For the El Salvador tsunami, the largest wave height was observed in Baltra, Galapagos Islands (71.1 cm) located about 1,400 km away from the source. The tsunami governing periods were around 9 and 19 min. Numerical modeling indicated that most of the tsunami energy was directed towards the Galapagos Islands, explaining the relatively large wave height there. For the Philippines tsunami, the maximum wave height of 30.5 cm was observed at Kushimoto in Japan located about 2,700 km away from the source. The tsunami governing periods were around 8, 12 and 29 min. Numerical modeling showed that a significant part of the far-field tsunami energy was directed towards the southern coast of Japan. Fourier and wavelet analyses as well as numerical modeling suggested that the dominant period of the first wave at stations normal to the fault strike is related to the fault width, while the period of the first wave at stations in the direction of fault strike is representative of the fault length.

Key words: Tsunami, earthquake, DART, tide gauge, spectral analysis, Fourier analysis, wavelet analysis, numerical modeling, El Salvador earthquake, Philippines earthquake.

1. Introduction

We studied two small tsunamis occurring in the Pacific basin in August 2012, generated by submarine earthquakes offshore El Salvador and Philippines (Fig. 1). According to the United States Geological Survey (USGS 2012a), the El Salvador earthquake occurred on 27 August 2012 at 04:37:20 GMT. The

epicenter of this M_w -7.3 earthquake was at 12.278°N and 88.528°W at the depth of around 20 km, producing almost no damage or casualty in the region (REUTERS 2012a). However, it generated a small tsunami in the Pacific Ocean whose wave amplitude was reported around 10 cm along the coastlines (CNN 2012a). A Field survey by BORRERO *et al.* (2014) showed that the tsunami generated a maximum runup of 6 m in the near-field, injuring several people. The first information bulletin about this tsunami was issued around 8 min after the earthquake occurrence, by the Pacific Tsunami Warning Center (PTWC) (PTWC 2012a). Following this early information, a tsunami warning was issued at 04:58 GMT (around 20 min after the earthquake) for the region (PTWC 2012b), and was cancelled around 110 min after the earthquake (PTWC 2012c).

The Philippines tsunami was slightly larger than the El Salvador one, having been produced by a slightly larger earthquake (M_w 7.6). According to the USGS (2012b), the origin time of the Philippines earthquake was at 12:47:34 GMT on 31 August 2012. The epicenter was at 10.838°N and 126.704°E at a depth of around 35 km (USGS 2012b). This offshore earthquake caused little damage and one death in the Philippines (REUTERS 2012b). Following this large submarine earthquake, a tsunami warning was issued at 12:55 GMT (around 8 min after the earthquake) for the region (PTWC 2012d). No damage was reported from the tsunami. Finally, the tsunami warning was cancelled at 14:54 GMT, about 2 h after the earthquake (PTWC 2012e).

In the following, we perform statistical, Fourier and wavelet analyses on the sea level records of these tsunamis in order to characterize the tsunami waves. In addition, numerical modeling of tsunami is conducted to give us insights into the propagation pattern of tsunami waves in the Pacific Basin.

¹ Earthquake Research Institute (ERI), The University of Tokyo, 1-1-1 Yayoi, Bunkyo-ku, Tokyo 113-0032, Japan. E-mail: mheidar@eri.u-tokyo.ac.jp

² Cluster of Excellence “The Future Ocean”, Christian-Albrechts University of Kiel, Kiel, Germany.

2. Sea level data

We report and analyze 25 sea level records of the aforesaid tsunamis consisting of both tide gauges and Deep-ocean Assessment and Reporting of Tsunamis (DART) records (Fig. 1; Tables 1, 2).

The sea level data were provided by the USA National Oceanographic and Atmospheric Administration (NOAA 2012) and the UNESCO Intergovernmental Oceanographic Commission (Ioc 2012). The sampling interval for all of the sea level data is 1 min.

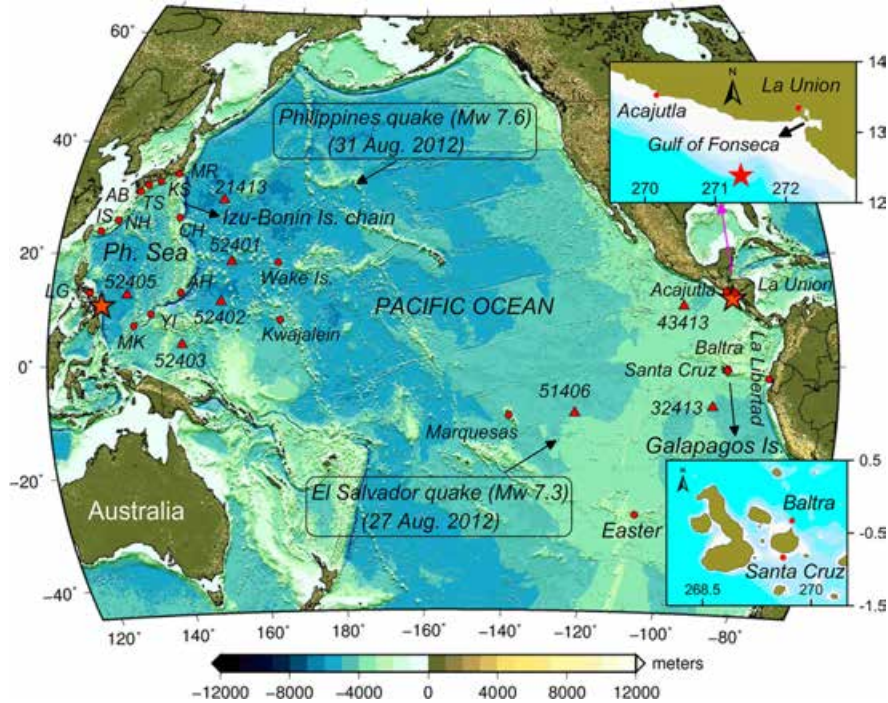


Figure 1

General location map of the Pacific Basin showing the locations of the El Salvador tsunami of 27 August 2012 (right asterisk) and the Philippines tsunami of 31 August 2012 (left asterisk). Solid circles and triangles represent the locations of tide gauge and DART stations, respectively. Abbreviations are: LG Legaspi, MK Malakal, YI Yap Island, AH Apra Harbor, IS Ishigakijima, NH Naha, TS Tosashimizu, AB Aburatsu, KS Kushimoto, CH Chichijima, MR Mera, and Ph. Sea Philippine Sea

Table 1

Sea level stations used to study the El Salvador tsunami of 27 August 2012

No.	Sea level station	Country (state)	Longitude	Latitude	Distance to the source (km)
Tide gauge stations					
1	La Union	El Salvador	87.82°W	13.31°N	140
2	Acajutla	El Salvador	89.84°W	13.57°N	206
3	Baltra	Ecuador	90.28°W	00.43°S	1,433
4	Santa Cruz	Ecuador	90.31°W	00.75°S	1,468
5	La Libertad	Ecuador	80.91°W	02.22°S	1,829
6	Easter	Chile	109.45°W	27.15°S	4,985
DART stations					
7	43413	SW of Acapulco, Mexico	99.85°W	11.07°N	1,271
8	32413	NW of Lima, Peru	93.50°W	07.40°S	2,267

Table 2

Sea level stations used to study the Philippines tsunami of 31 August 2012

No.	Sea level station	Country (state)	Longitude	Latitude	Distance to the source (km)
Tide gauge stations					
1	Legaspi	Philippines (Albay)	123.76°E	13.15°N	417
2	Malakal	Palau Islands	134.45°E	07.33°N	949
3	Yap Island	Micronesia	138.12°E	09.51°N	1,283
4	Ishigakijima	Japan (Okinawa)	124.10°E	24.20°N	1,520
5	Naha	Japan (Okinawa)	127.67°E	26.22°N	1,721
6	Aburatsu	Japan	131.41°E	31.58°N	2,376
7	Chichijima	Japan	142.19°E	27.09°N	2,507
8	Tosashimizu	Japan (Kochi)	132.97°E	32.78°N	2,548
9	Kushimoto	Japan	135.77°E	33.48°N	2,724
10	Mera	Japan	139.83°E	34.92°N	3,063
11	Wake Island	USA (Wake Island)	166.62°E	19.28°N	4,557
12	Kwajalein	Marshall Islands	167.73°E	08.73°N	4,588
DART stations					
13	52405	West of Pacific Ocean, Guam	132.33°E	12.88°N	669
14	52403	West of Pacific Ocean, Truk	145.59°E	04.05°N	2,241
15	52402	NW of Kwajalein	154.04°E	11.87°N	3,055
16	52401	NE of Saipan	155.77°E	19.26°N	3,380
17	21413	SE of Tokyo, Japan	152.12°E	30.52°N	3,590

3. Methods of Waveform Analyses

3.1. Tsunami Waveform Detection

The following steps were employed to detect the tsunami signal from the sea level records: (1) quality control, and (2) removing low-frequency signals like tides by high-pass filtering. The Butterworth IIR digital filter (MATHWORKS 2012) was employed to remove low frequency signals for which a cut-off frequency of 0.0003 Hz (about 1 h) was chosen. To examine whether the Butterworth digital filter generates a spurious leading depression wave or not in our analyses, we performed tidal harmonic analysis for selected waveforms (Sect. 4.1).

3.2. Statistical Analysis

We calculated the following physical parameters of the tsunami (HEIDARZADEH and SATAKE 2013a): (1) the arrival time of the first tsunami wave, (2) the polarity of the first wave, (3) the arrival time of the maximum wave, (4) the maximum trough-to-crest wave height, (5) the number of waves before the arrival of the maximum wave, and (6) duration of tsunami.

3.3. Spectral Analysis

The spectral content of a tsunami record is mostly dictated by two factors: (1) the effect of local and regional bathymetric features like continental shelves and coastal harbors/bays, and (2) the effect of tsunami source and dimensions of the seafloor deformation. In this context, a tide gauge record of a tsunami usually includes both of the aforesaid effects, because tide gauges are deployed in coastal areas and hence bathymetric features play an important role in their records. In contrast, DART records mostly reflect tsunami source characteristics, as they are deep-water instruments and hence are free from shallow bathymetric effects. To separate tsunami source and bathymetric effects in a tide gauge record, RABINOVICH (1997) proposed to compare spectral peaks computed from tsunami water level data recorded at different locations and then to pick the common spectral peaks contained within different water level spectra from a particular tsunami. We applied this method to separate source and bathymetric effects in our tide gauge data. In this study, we applied two methods to investigate the spectral content of the tsunami signals: Fourier and wavelet analyses.

3.3.1 Fourier Analysis

For Fourier analysis, we used Welch's averaged-modified-periodogram method of spectral estimation by considering Hamming window and overlaps (WELCH 1967). Calculation of the signal spectrum was done using the Welch algorithm from the signal processing toolbox in Matlab program (MATHWORKS 2012).

3.3.2 Wavelet Analysis

Wavelet analysis, also known as the frequency-time ($f-t$) analysis, has been used in tsunami research for studying the temporal changes of tsunami energy (RABINOVICH and THOMSON 2007; HEIDARZADEH and SATAKE 2013a; BORRERO and GREER 2013). Since a tsunami is a non-stationary signal, its spectral content varies in strength and peak frequency over time. Wavelet analysis presents the distribution of tsunami energy in different frequency bands (f) over time (t). In other words, wavelet analysis shows in which period band tsunami energy is concentrated at a particular time, and hence can be considered as a complementary analysis for Fourier analysis. Because a tsunami is a non-stationary signal, the use of wavelet analysis allows for the analysis of the frequency content of a tsunami wave train as it changes over time. More details about wavelet analysis is given in TORRENCE and COMPO (1998) and HEIDARZADEH and SATAKE (2013a, b).

4. Results of the Analyses

4.1. Tsunami Waveforms

Figure 2 presents the original and filtered signals for the El Salvador tsunami of 27 August 2012 (Fig. 2a) and the Philippines tsunami of 31 August 2012 (Fig. 2b, c). It can be seen that the tsunami signal is clear in most of the analyzed tide gauge records. The El Salvador tsunami was recorded on five coastal tide gauges and two DART stations (DARTs 43413 and 32413). The Philippine tsunami was recorded on ten coastal tide gauges and on two DART stations of 52405 and 52403 with 1-min temporal resolution. While the tsunami was possibly

recorded on DART stations 52402, 52401 and 21413, the tsunami arrival occurred after the station had been switched from 1-min sampling to 15 min sampling. Under-sampled traces of seismic waves are also present in the DART records of both events and are evident in the figures.

Figure 2d compares the results of Butterworth digital filter (middle panel) with those of tidal harmonic analysis (right panel) for four stations recording the Philippines tsunami. We applied the tidal analysis package Tidal Analysis Software Kit (TASK) for tidal analysis (BELL *et al.* 2000). Figure 2d shows that both of the analyses yield almost the same results, indicating that the applied digital filter is not producing spurious leading depression waves.

4.2. Statistical Properties of the Tsunamis

Based on the filtered tsunami signals (Fig. 2), the main physical properties are summarized in Tables 3 and 4.

4.2.1 El Salvador Tsunami

Among the analyzed sea level stations for the El Salvador tsunami, the Acajutla tide gauge was the first one to receive the tsunami. The first arrival in La Union can be distinguished by taking into consideration the fact that the period of tsunami is larger than that of noise signals. The time interval between the first tsunami peak (asterisk in Fig. 2a) and the next peak is around 16 min for the La Union record. It will be shown later that the 16-min signal is one of the governing signals of the El Salvador tsunami. The largest trough-to-crest wave height is 71.1 cm recorded at the Baltra tide gauge station at a distance of around 1,400 km from the tsunami source (Table 3). At other far-field stations like Santa Cruz and La Libertad, wave heights of 34.4 and 35.6 cm were recorded, respectively, though the Santa Cruz station is located in the far-field on the lee side of the Galapagos island system relative to the direction of incidence of the tsunami (Fig. 1). The far-field wave heights are about five times larger than the near-field wave heights (e.g., La Union station). Comparison of average values for the DART and tide gauge

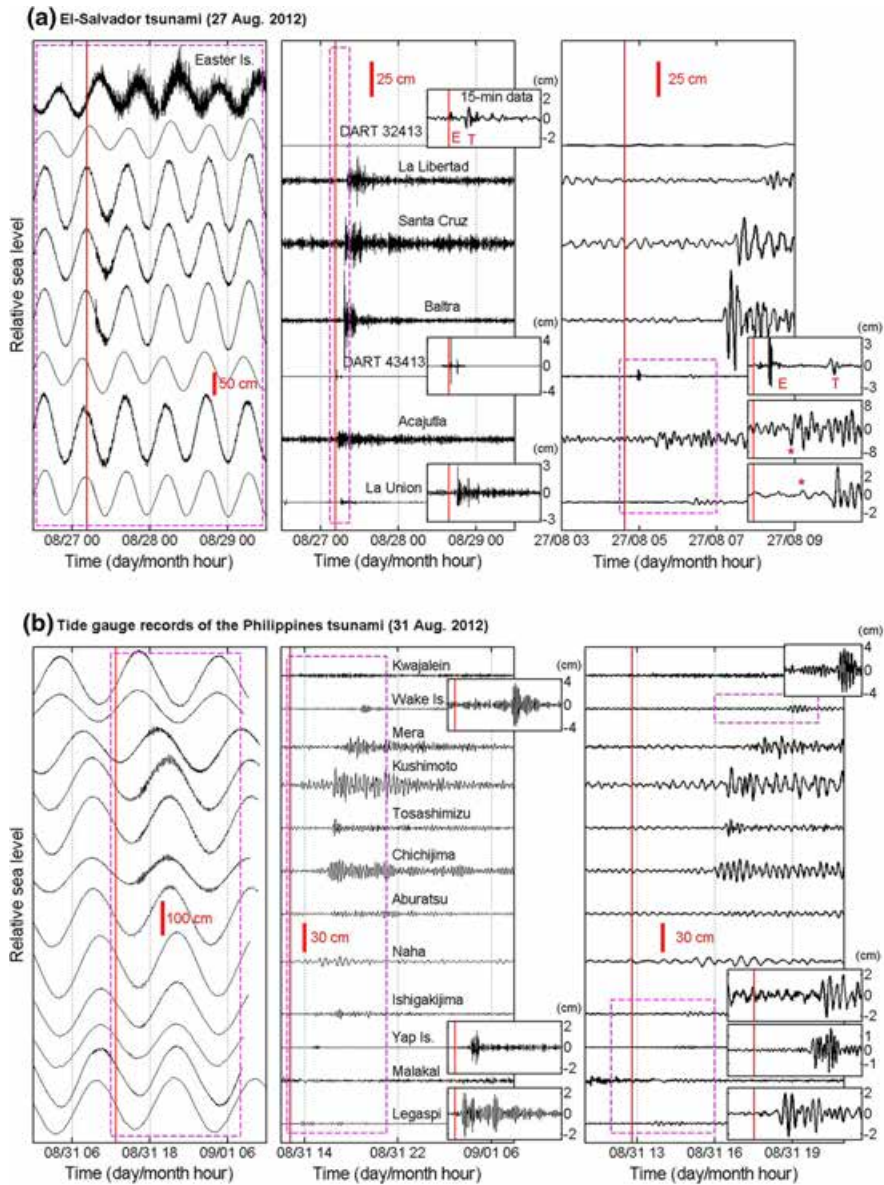


Figure 2

Sea level records of the El Salvador tsunami of 27 August 2012 (a) and the Philippines tsunami of 31 August 2012 (b, c). The *left* and *middle* panels show the original and filtered signals, respectively. In the *right* panel, only a small part of the filtered signal is enlarged. The letters *E* and *T* represent Earthquake and Tsunami, respectively. The *dashed rectangle* shows part of the data enlarged in the neighboring panel. *Small insets* show the respective waveforms with a better resolution. *Asterisks* show the arrival times of the first wave. **d** Comparison of the results of waveform analysis performed by the Butterworth digital filter (*middle panel*) and the tidal harmonic analysis (*right panel*). Tide predictions are shown by *blue curves* in the *left panel*. The *red-vertical line* represent the time of the earthquake occurrence

waveforms (Table 3) indicate three main differences between tsunami records on DARTs and tide gauges: (1) Duration of tsunami oscillations on tide gauges is about four times longer than that on DARTs, (2) the

maximum wave height on tide gauges is 14 times larger than that on DARTs, and (3) the first wave is the largest one in DART records, whereas the second, third or later wave is the largest in tide gauge records.

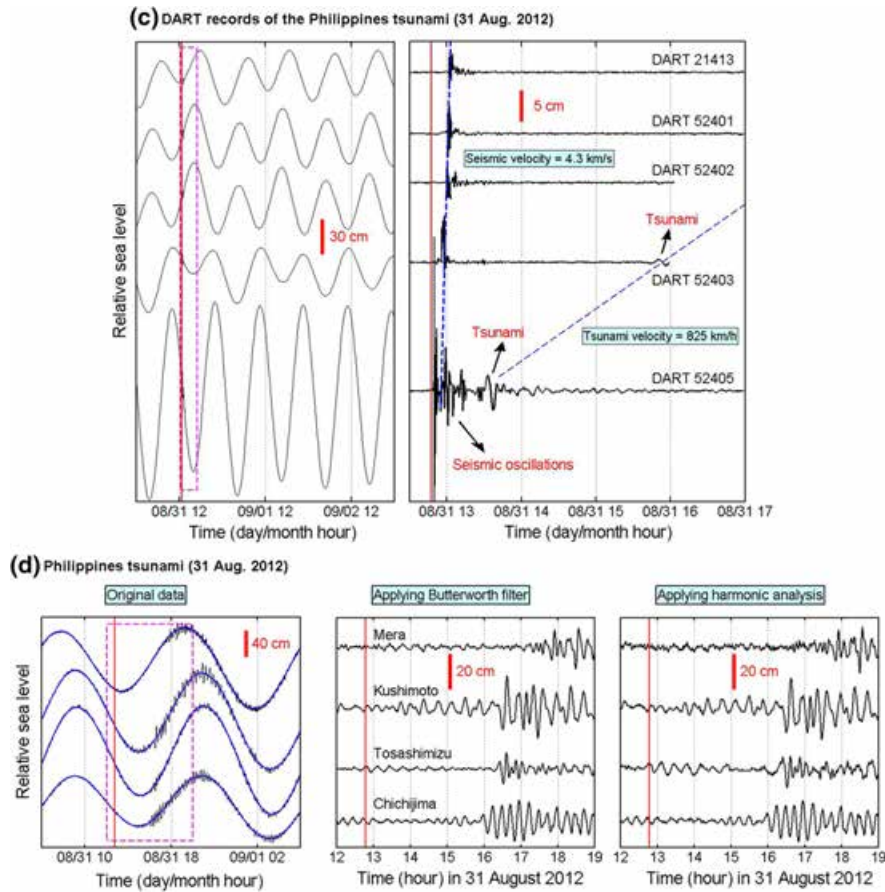


Figure 2 continued

4.2.2 Philippines Tsunami

The largest wave height was 30.5 cm, recorded at Kushimoto (Japan) for the Philippines tsunami. Similar to the El Salvador tsunami, among the analyzed sea level stations for the Philippines tsunami (Table 4), the near-field wave heights are significantly smaller than the far-field ones. According to Table 4, deep water tsunami waves recorded at DART 52405 have smaller amplitudes and last for a shorter time compared to those recorded by tide gauges.

4.3. Spectral Peaks

Fourier analysis of the tsunami waveforms identified a few peaks, which are shown by asterisks in

Fig. 3 and are summarized in Tables 5, 6. We performed Fourier analysis for both the entire tsunami waveform (Fig. 3/left panels) and for the first 2 h (Fig. 3/right panels), and then the peak periods were picked from the latter spectra. It is expected that the 2-h-long spectra are less influenced by coastal bathymetric features. In general, a clear difference can be seen between the tsunami spectra of DARTs and those of tide gauges. Tsunami spectrum is usually simple and consists of only one peak for DARTs, whereas it is relatively complicated and includes several peaks for tide gauges.

4.3.1 El Salvador Tsunami

The analysis suggests spectral peaks at approximately 19 and 9 min for the El Salvador tsunami (Fig. 3a;

Table 3
Statistical properties of the El Salvador tsunami of 27 August 2012

No.	Sea level station	First wave			Maximum wave			Duration (h)
		Arrival time (GMT) (dd/mm-HH:MM)	Travel time ^a (h:min)	Sign ^b	Arrival time (GMT) dd/mm-HH:MM)	Travel time ^a (h:min)	Observed max. wave height (cm) ^c	
1	La Union	27/08-05:39	01:02	(+)	27/08-06:11	01:34	4.5	3
2	Acajutla	27/08-05:23	00:46	(-)	27/08-09:29	04:52	12.5	23
3	Baltra	27/08-07:08	02:31	(+)	27/08-07:21	02:44	71.1	2
4	Santa Cruz	27/08-07:25	02:48	(+)	27/08-07:34	02:57	34.4	2
5	La Libertad	27/08-08:11	03:44	(+)	27/08-11:23	06:46	35.6	17
6	Easter	NA ^d	NA	NA	NA	NA	NA	NA
Average								
7	DART 43413	27/08-06:15	01:38	(+)	27/08-06:19	01:42	31.6	9
8	DART 32413	NA	NA	NA	27/08-08:15	03:38	2.3	1
Average							2.2	1
							2.25	1

^a Compared to the earthquake origin time (27/08/2012 04:37:20^{''} GMT)

^b (-) and (+) represent leading depression and elevation waves, respectively

^c Maximum trough-to-crest wave height

^d Not Applicable

Table 4
Statistical properties of the Philippines tsunami of 31 August 2012

No.	Sea level station	First wave			Maximum wave			Duration (h)
		Arrival time (GMT) (dd/mm-HH:MM)	Travel time ^a (h:min)	Sign ^b	Arrival time (GMT) (dd/mm-HH:MM)	Travel time ^a (h:min)	Observed max. wave height (cm) ^c	
1	Legaspi	31/08-13:23	00:36	(+)	31/08-13:43	00:56	4.2	2
2	Malakal	NA ^d	NA	NA	NA	NA	NA	NA
3	Yap Island	31/08-14:28	01:41	(+)	31/08-15:04	02:17	3.2	6
4	Ishigakijima	31/08-14:45	01:58	(+)	31/08-16:59	04:12	9.8	11
5	Naha	31/08-15:05	02:18	(+)	31/08-17:00	04:13	10.5	5
6	Aburatsu	NA	NA	NA	31/08-20:53	08:06	7.3	NA
7	Chichijima	31/08-15:52	03:07	(+)	31/08-16:57	04:10	24	5
8	Tosashimizu	31/08-16:19	03:32	(+)	31/08-16:37	03:50	17.9	2
9	Kushimoto	31/08-16:25	03:38	(+)	31/08-16:38	03:51	30.5	2
10	Mera	31/08-17:36	04:49	(+)	31/08-18:34	05:47	23.9	5
11	Wake Island	31/08-18:36	05:49	(+)	31/08-19:05	06:18	7.5	3
12	Kwajalein	NA	NA	NA	NA	NA	NA	NA
Average							13.9	5
13	DART 52405	31/08-13:31	00:44	(+)	31/08-13:33	00:46	5.8	1
14	DART 52403	31/08-15:50	03:03	(+)	31/08-15:50	03:03	1.01	1

^a Compared to the earthquake origin time (31/08/2012 12:47:34" GMT)

^b (-) and (+) represent leading depression and elevation waves, respectively

^c Maximum trough-to-crest wave height

^d Not applicable

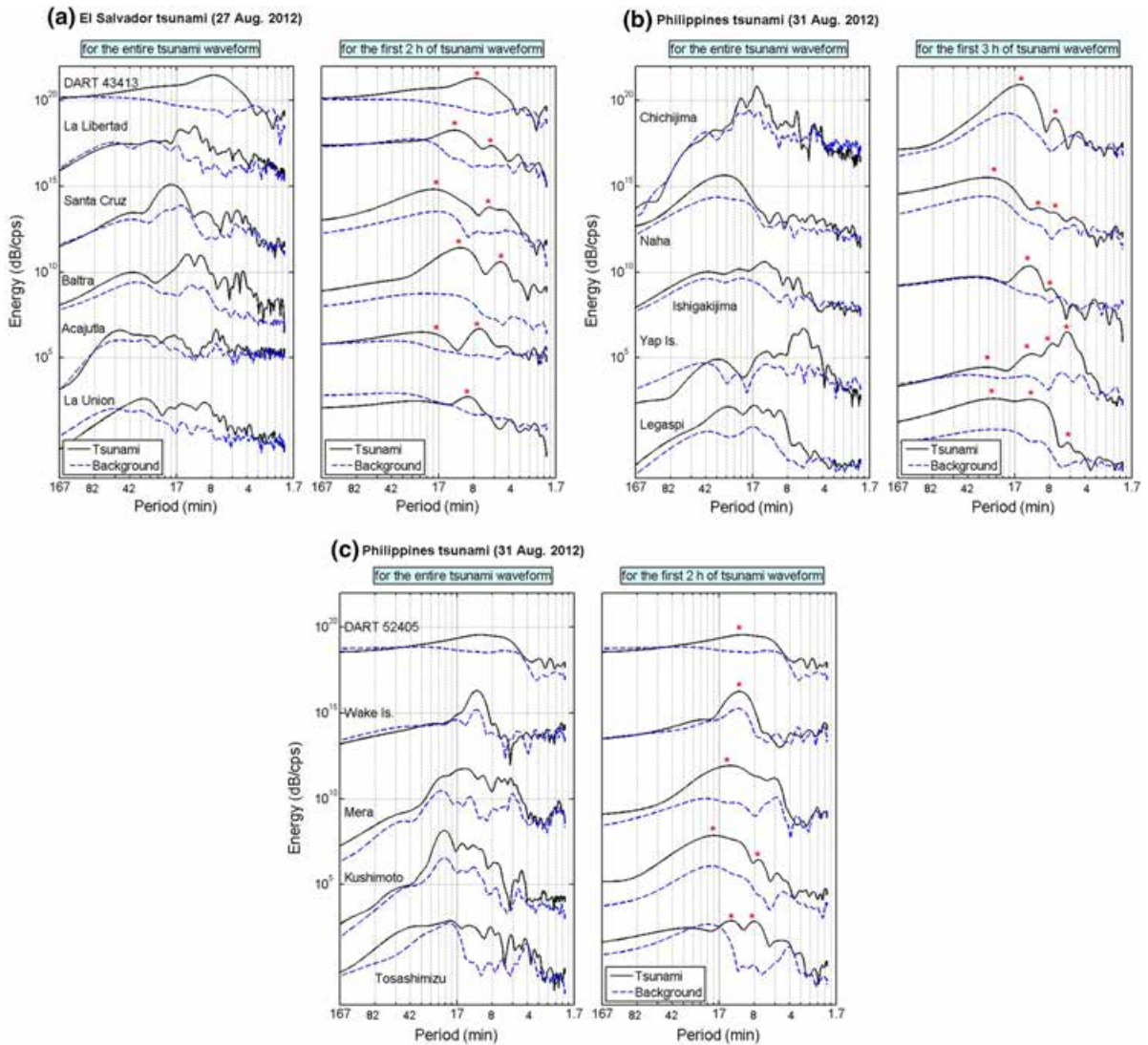


Figure 3

Spectra for the sea level records of the El Salvador tsunami of 27 August 2012 (a) and the Philippines tsunami of 31 August 2012 (b, c). Fourier analysis is performed for both the entire tsunami waveforms (left panels) and for the first 2 h of the tsunami waveforms (right panels). Asterisks show some of the peak periods in each spectrum. Solid and dashed lines show the spectra of tsunami and background signals, respectively

Table 5); these are possibly the main tsunami source periods. The most governing signal is possibly the one with the period of around 9 min, because this signal is the one that is most common in Table 5.

4.3.2 Philippines Tsunami

For the Philippines tsunami, the governing periods are 29, 12, and 8 min (Fig. 3b, c; Table 6), among which the 12-min period seems to be the strongest

one because it is the most common signal in different stations (Table 6). The period of the tsunami recorded at the DART 52403 is also 12 min (Fig. 2c). Some unusual observations can be seen in the tsunami spectra shown in Fig. 3b, c. For example, during the Philippines tsunami, the most powerful signal is the 5.9-min signal in Yap Island, whereas either 29- or 12-min signals are the governing ones in all of the other stations. The 5.9-min period is possibly one of the resonance modes

Table 5

Governing periods of the El Salvador tsunami of 27 August 2012 based on the spectra of the first 2 h of the tsunami waveforms (Fig. 3a/right panel)

No.	Station	Peak periods (min)
1	La Union	9.4
2	Acajutla	19.3, 7.5
3	DART 43413	7.9
4	Baltra	10.8, 4.9
5	Santa Cruz	18.5, 6.2
6	La Libertad	12.2, 5.9

Table 6

Governing periods of the Philippines tsunami of 31 August 2012 based on the spectra of the first 2 h of the tsunami waveforms (Fig. 3b, c/right panel)

No.	Station	Peak periods (min)
1	Legaspi	25.6, 12.4, 5.9
2	Yap Island	28.9, 11.8, 7.9, 5.9
3	Ishigakijima	12.5, 8.2
4	Naha	28.9, 10.4, 7.8
5	Chichijima	15.0, 7.5
6	Tosashimizu	13.1, 8.3
7	Kushimoto	18.3, 7.7
8	Mera	13.2
9	Wake Island	11.1
10	DART 52405	10.4

of the harbor/bay, in which the Yap Island tide gauge is located.

4.4. Temporal Changes of Dominant Periods

Wavelet analyses for the sea level records of the El Salvador and Philippines tsunamis are shown in Fig. 4, as is the global wavelet spectrum, which is the time-averaged spectral energy over all times. It should be noted that Fourier analysis (Fig. 3) gives the power of signals with different periods over the entire tsunami record, whereas wavelet analysis gives the time evolution of wave energy. Hence, the Fourier analysis given by global wavelet spectrum (Fig. 4) is slightly different from that of normal Fourier analysis performed by Welch algorithm (Fig. 3). This is why there are differences between the amount of peak energy given by Fourier (Fig. 3) and wavelet analyses (Fig. 4) although the peak periods are almost the same in both.

4.4.1 El Salvador Tsunami

For the El Salvador tsunami recorded at Santa Cruz, most of the tsunami energy is distributed in the narrow period band of 11–24 min over the entire tsunami oscillations. The Acajutla's $f-t$ plot shows that the level of wave energy before the earthquake occurrence is as high as that after the earthquake for the period band of around 45 min, indicating that this period band cannot be attributed to the tsunami. There is almost no energy at the period bands of around 7–10 and 18–20 min before the earthquake occurrence, whereas the wave energy at these period bands is higher after the earthquake. This indicates that both of the aforesaid periods may belong to the tsunami. On the other hand, we may conclude that the peak period of 45 min at the La Libertad station (Fig. 4a) belongs to non-tsunami sources (e.g., local and regional bathymetric effects).

4.4.2 Philippines Tsunami

Based on the $f-t$ plots for the Philippines tsunami (Fig. 4b, c), it can be seen that most of the wave energy is distributed at three different period bands of around 10–13, 25–30, and 45 min. However, the period band of 45 min most probably belongs to non-tsunami sources, because the level of energy in this band is high before the arrival of tsunami in many of the examined stations. This idea is supported by the tsunami and background spectra shown in Fig. 3b, c because the levels of energy in both spectra are almost the same around the period of 45 min. Distinct wave trains with high energy contents are clear at Naha. According to the wavelet plot of the Ishigakijima record (Fig. 4b), by neglecting the 45-min signal, the governing period of tsunami is around 10–12 min for the first few hours after the tsunami arrival; then the governing period switches to the period of around 20–28 min. On the contrary, the 28-min signal is the first signal arriving at the Legaspi station (Fig. 4b). At Wake Island (Fig. 4c), most of the tsunami energy occurs at the period of around 10–12 min and almost no energy is present at the period band of 20–28 min. For Mera (Fig. 4c),

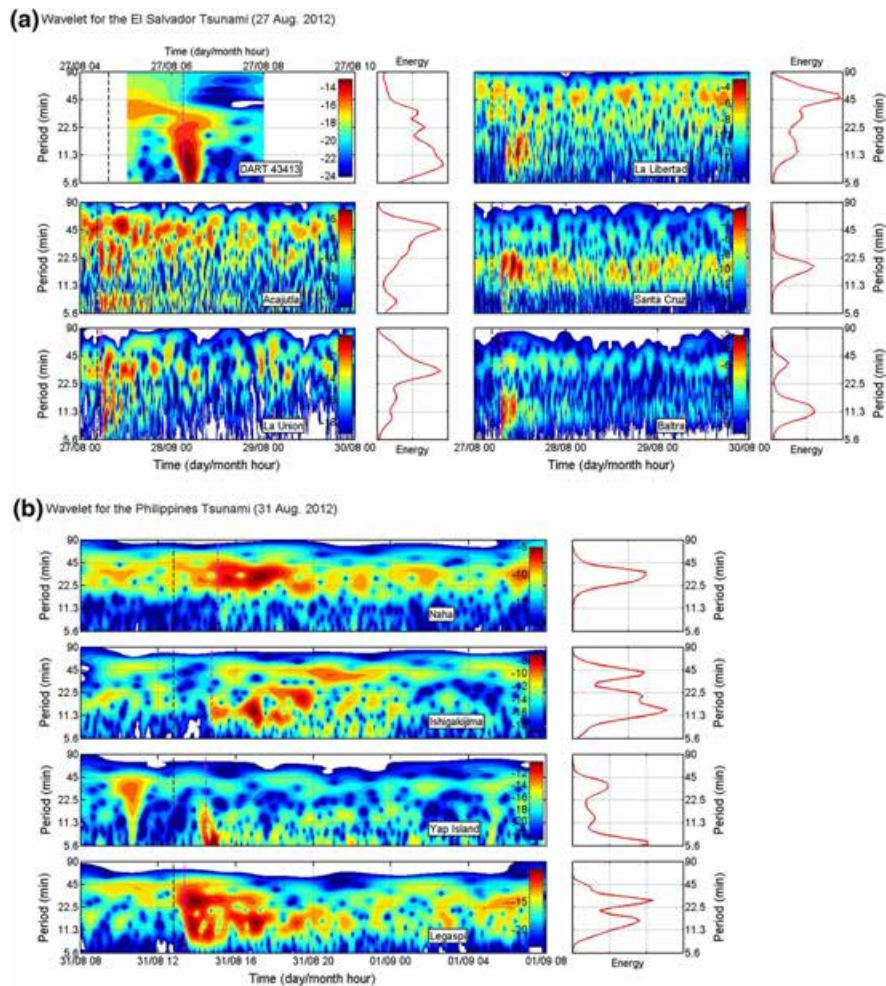


Figure 4

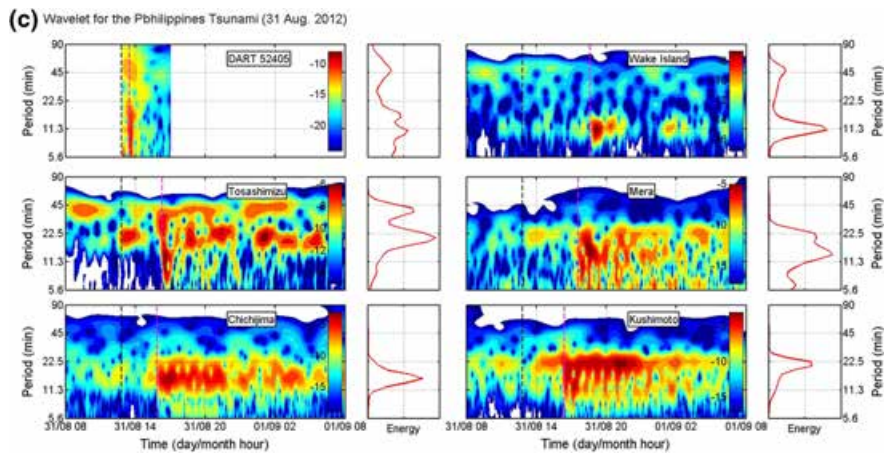
Wavelet analysis for the sea level records of the El Salvador tsunami of 27 August 2012 (a) and the Philippines tsunami of 31 August 2012 (b, c). *Dashed-vertical dark and purple lines* represents the earthquake occurrence and tsunami arrival times, respectively. The *small plots*, at the *right side* of each wavelet plot, show the global wavelet spectrum

tsunami energy is distributed over a wide period band of 5–25 min. The governing period is around 10–15 min for Chichijima, while it is around 20–25 min for Kushimoto (Fig. 4c).

4.5. Summary of the Sea Level Data Analysis

The analysis of the El Salvador and Philippines tsunamis of August 2012 using sea level data showed some unusual observations, such as: (1) for the El Salvador tsunami, relatively large wave height of 34.4 cm was observed on the lee side of the Galapagos

island system relative to the direction of incidence of the tsunami; (2) although the Philippines earthquake (M_w 7.6) was larger than the El Salvador one (M_w 7.3), the maximum wave height generated by the El Salvador tsunami was almost two times bigger than that generated by the Philippines tsunami; (3) the largest wave heights produced by the Philippines tsunami were observed in the far-field especially along the Japan coast; and (4) the largest wave heights of the El Salvador tsunami occurred in the far-field. We perform numerical modeling of both tsunamis in order to shed some light on the above unusual observations.

Figure 4
continued

5. Numerical Modeling of Tsunami Waves and Validation

5.1. Method and Validation

The analytical formulas by OKADA (1985) were employed to calculate the seafloor deformation due to the parent earthquake using the seismic parameters of the earthquake. The earthquake fault parameters are taken from the GLOBAL CMT (2012) and the USGS centroid moment solution (USGS 2012a, b) summarized in Table 7. Figure 5a shows the result of the seafloor deformation modeling. The 1-min bathymetry grid provided through the GEBCO digital atlas was used here for numerical modeling of tsunami (Ioc *et al.* 2003). The numerical model used here is the same as that described in YALCINER *et al.* (2004), solving non-linear shallow water equations using a leap frog scheme on a staggered grid system. A time step of 3.0 s is applied and tsunami inundation on dry land is not included.

To validate the results of tsunami modeling, we compare time histories of the simulated waves with actual ones observed on DARTs and tide gauges. Figure 5b presents the results of this comparison, in which five actual sea level records are compared with the simulated ones for each tsunami. Although the grid spacing is 1 min, good agreement can be seen between the simulated and observed waveforms. The agreement is highly satisfactory for DART records. In Legaspi, the discrepancy between the observed and

simulated wave height is relatively large; however, the arrival times are almost the same. It seems that the tsunami simulations performed here are accurate enough for this study, which is aimed at studying the propagation pattern of the two tsunamis.

5.2. The El Salvador Tsunami

Snapshots of the El Salvador tsunami in Fig. 6a show that tsunami waves experience two major reflections from Isla-Del-Coco and the Galapagos Islands, which occur about 1.5 and 2.5 h after the earthquake, respectively. It is clear from Fig. 6a that each reflection acts as a new source for tsunami waves, introducing new wave trains into the tsunami wave field. Late wave trains in tsunami waveforms (Fig. 2) may be attributed to these reflected waves that arrive some hours after the earthquake generation. It is long known that a tsunami is a series of long waves; not a single wave. This is clear from the snapshot of the El Salvador tsunami at the time of 3 h (Fig. 6a) where a chain of successive wave crests (C) and troughs (T) can be seen.

Figure 6c shows the distribution of the maximum wave height of the El Salvador tsunami. Most of the tsunami energy is directed towards the Galapagos Islands. This is due to the directivity of tsunami waves in the far-field. Proposed by BEN-MENAHEN and ROSENMAN (1972), directivity of tsunami indicates that most of the tsunami energy travels

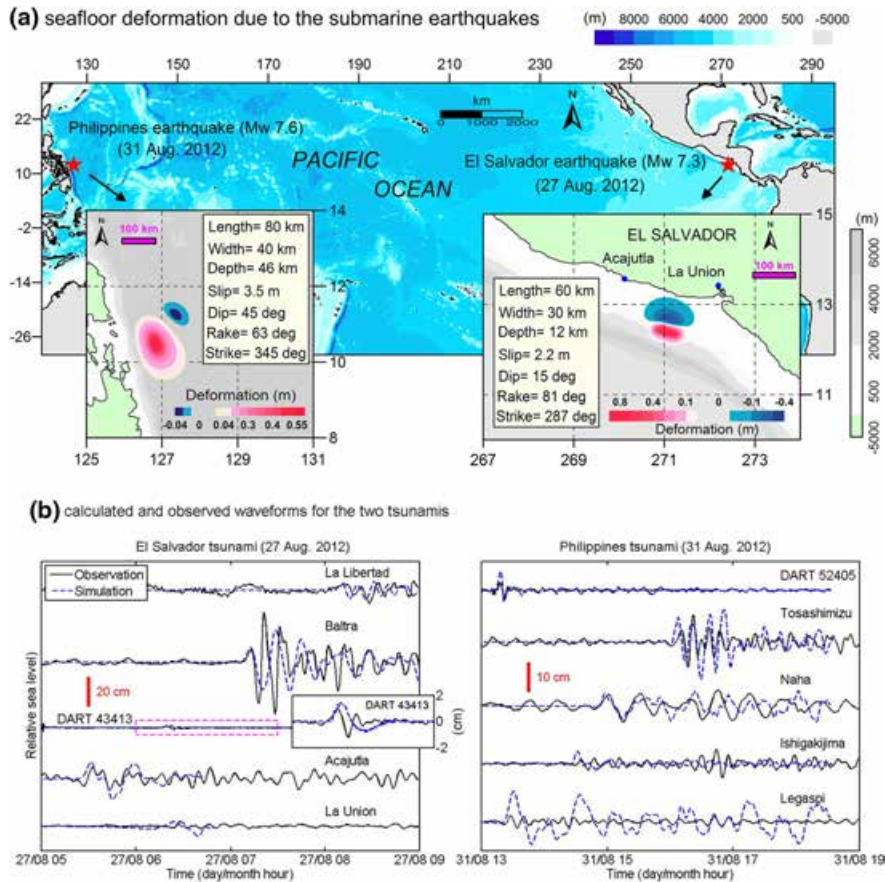


Figure 5

Results of numerical modeling of tsunami. **a** Seafloor deformation due to the El Salvador and Philippines tsunamis. Numbers on axes are in degrees. *Asterisks* show the epicenters of the earthquake. **b** Simulated and observed waveforms for the two tsunamis

perpendicular to the source strike in the far-field. Considering that the strike of the fault responsible for the El Salvador tsunami is SE–NW (Fig. 5a), the largest tsunami waves travel in the NE–SW direction (Fig. 6c). Hence, observation of the maximum wave height of the El Salvador tsunami at the Baltra station can be explained by the directivity effect. Snapshots of the El Salvador tsunami simulation around the Santa Cruz station (Fig. 6d) reveal that two different waves arrived almost at the same time from opposite sides, and are superpositioned into a single wave. One wave train comes from around the Isabela Island to the west and another wave train from the east side of the Santa Cruz Island. This phenomenon may explain the relatively large wave height of around 35 cm in Santa Cruz.

5.3. The Philippines Tsunami

Snapshots of the Philippines tsunami in Fig. 6b reveal that the tsunami wave field is more complicated than that of the El Salvador tsunami; this can be attributed to the presence of the Izu-Bonin Island chain and other Pacific Islands around the tsunami source area. Tsunami waves are reflected from this island chain and can hardly exit the Philippine Sea region. This is also supported by Fig. 6c, where the distribution of the maximum wave height of tsunami is presented. Figure 6c reveals that most of the tsunami energy is confined within the Philippine Sea region and only a small part of the tsunami is able to exit from the Philippine Sea.

The other fact in Fig. 6c is that a significant part of the Philippines tsunami energy is directed towards the

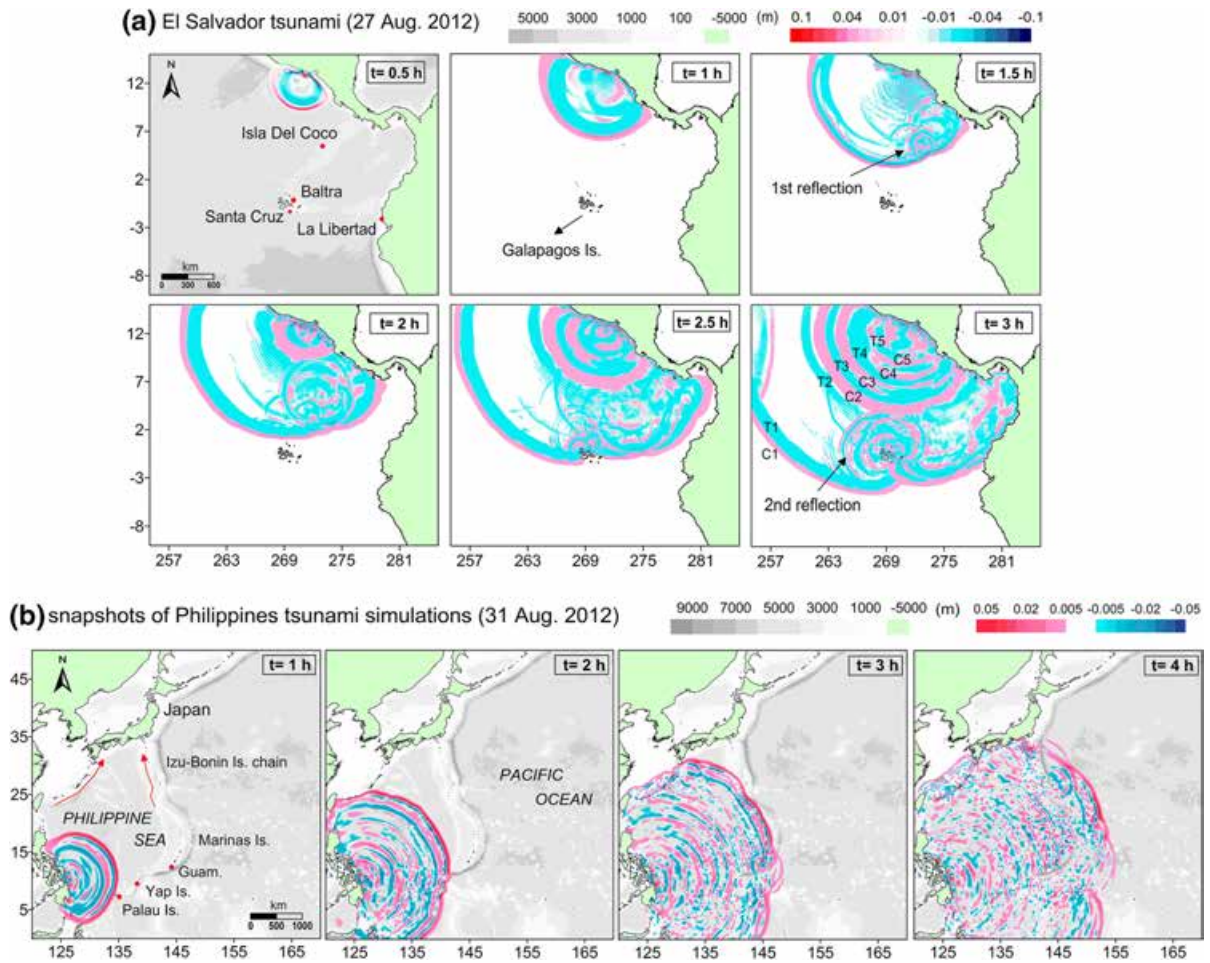


Figure 6

Results of numerical modeling of tsunamis. **a** Snapshots of tsunami simulations for the El Salvador tsunami. *C* and *T* represent crest and trough waves, respectively. **b** Snapshots of tsunami simulations for the Philippines tsunami. **c** Distribution of the maximum wave amplitudes of tsunami for the two tsunamis. **d** Snapshots of the El Salvador tsunami around the Santa Cruz station. Numbers on axes are in degrees

southern coast of Japan (arrow B in Fig. 6c). In fact, the energy of the Philippines tsunami is partitioned into two parts: (1) the first part of tsunami energy travels perpendicular to the source strike (arrow A in Fig. 6c), which can be explained by the directivity effect; and (2) the second part travels towards the southern coast of Japan (arrow B in Fig. 6c), which can be explained by the effect of bathymetry on far-field propagation of tsunamis proposed by SATAKE (1988). Arrows in Fig. 6b show how the Izu-Bonin Island chain funnels the tsunami waves towards southern Japan. Observation of relatively large wave heights in Japanese coastlines due to the Philippines tsunami may be explained by this effect.

5.4. Comparing the Two Tsunamis

According to Tables 3 and 4, among the examined sea level records, the average wave height produced by the El Salvador tsunami is about two times larger than that produced by the Philippines tsunami, although the former earthquake (M_w 7.3) was smaller than the latter earthquake (M_w 7.6). The El Salvador earthquake was more efficient for tsunami generation than the Philippines one for three reasons. First, the former earthquake occurred at a shallower depth. Second, the former earthquake has a larger dip-slip component, although the dip angle is smaller (Table 7). Due to these reasons, the maximum

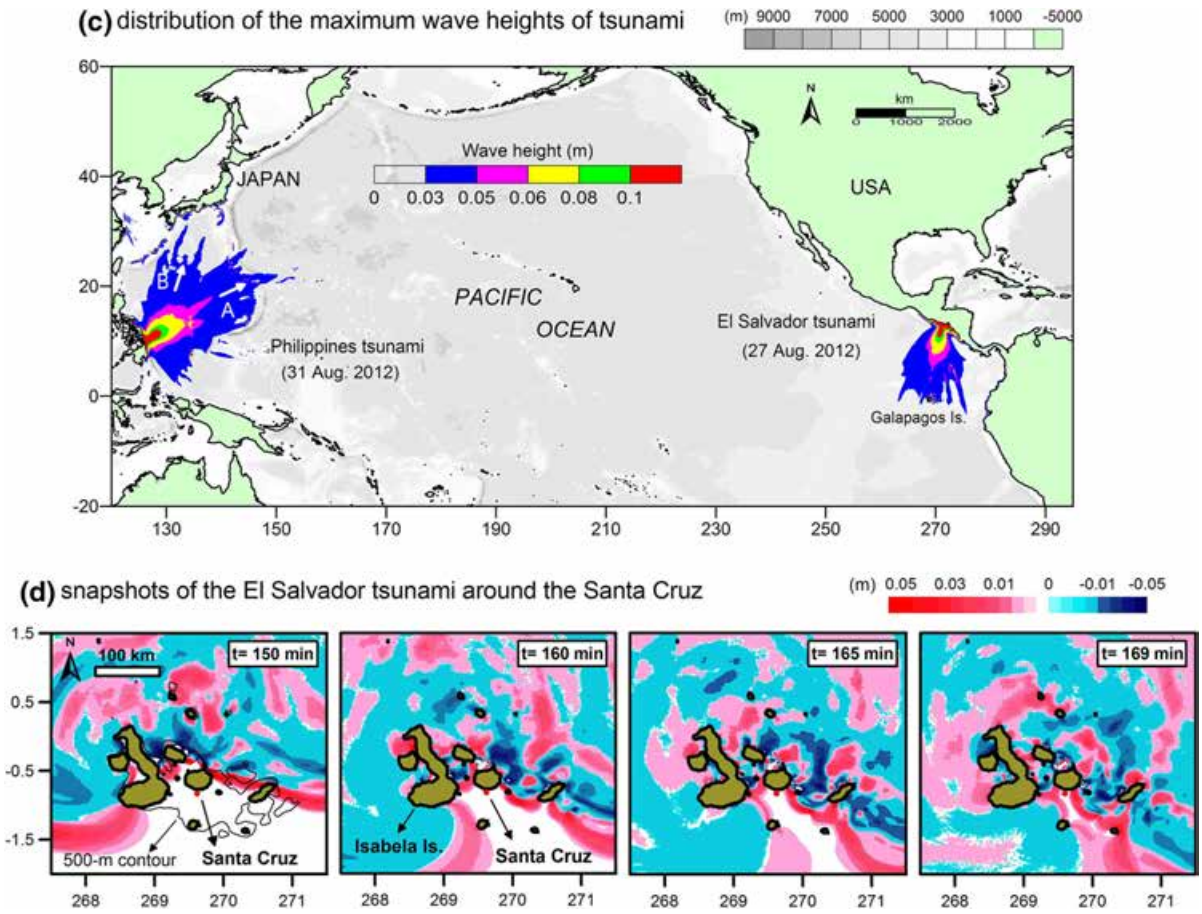


Figure 6 continued

seafloor uplift due to the El Salvador earthquake is larger than that of the Philippines earthquake (Fig. 5a). It is evident that the larger the seafloor uplift is, the stronger the tsunami. Third, based on the source-time functions of both earthquakes shown in

Fig. 7, the El Salvador earthquake was a slow earthquake. The source duration of the El Salvador earthquake was around 70 s; this is comparable to some other slow-tsunamigenic earthquakes (known as “tsunami earthquakes”), like the 1992 Nicaragua

Table 7

Tectonic parameters used for modeling seafloor deformation at the tsunami source according to GLOBAL CMT (2012) and the USGS (2012a, b)

Event name	M_0^a (dyn. cm)	M_w^b	Fault start point		Fault end point		Length (km)	Width (km)	Slip (m)	Depth (km)	Dip (deg)	Rake (deg)	Strike (deg)
			Lon (°)	Lat (°)	Lon (°)	Lat (°)							
El Salvador (27 Aug 2012)	1.18×10^{27}	7.3	88.70 (°W)	12.3 (°N)	89.22 (°W)	12.46 (°N)	60	30	2.2	12	15	81	287
Philippines (31 Aug 2012)	3.34×10^{27}	7.6	126.80 (°E)	10.20 (°N)	126.63 (°E)	10.90 (°N)	80	40	3.5	46	45	63	345

^a Seismic moment

^b Moment magnitude

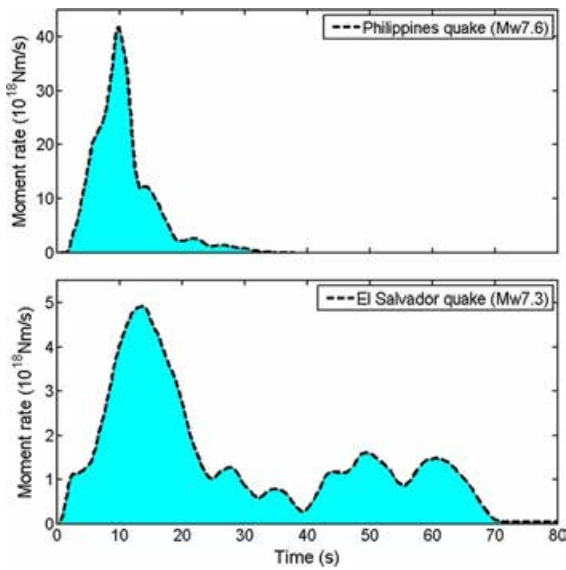


Figure 7

Source-time functions for the two earthquakes of El Salvador (27 August 2012-Mw 7.3) and Philippines (31 August 2012-Mw 7.6).

The data is from the finite fault model of USGS (2012a, b)

earthquake (KANAMORI and KIKUCHI 1993) and the 2010 Mentawai earthquake (SATAKE *et al.* 2013). Slow earthquakes have been reported to be more efficient in tsunami generation than ordinary ones.

6. Discussions

6.1. Insights into the Tsunami Source Dimension Using Wavelet Analysis

It is already known that the main governing periods of tsunamis are normally dictated by the dimensions of the earthquake fault (i.e., length/width), as schematically shown for the Philippines tsunami in Fig. 8 (HEIDARZADEH and SATAKE 2013a). The sea level stations located normal to the fault strike (e.g., Wake Is. in Fig. 8) are mainly influenced by the tsunami period determined by the source width. For other stations located at different sides of the tsunami source (i.e., the lateral stations like Legaspi in Fig. 8), the tsunami signal controlled by the source length is usually the first wave to arrive at these stations. As most of the tsunami energy is usually concentrated towards normal to the source strike (i.e., directivity effect), the period of tsunami is mainly controlled by the width of the source rupture.

Therefore, even for the stations receiving first waves imposed by the source length, we may expect that the governing tsunami signal is the one imposed by the source width. However, any connection between a certain period and the width/length of the source fault needs to be made cautiously, because a tsunami spectrum usually shows multiple peaks due to the various local/regional/global bathymetric features. In fact, the periods dictated by the source fault are mixed with other periods imposed by bathymetric effects. In addition, the aforesaid connection between source dimensions and tsunami governing periods is a general rule and we may not expect it to hold true for every tsunami waveform, as tsunami source is, in reality, a heterogeneous one and tsunami waveforms are affected by several factors.

The Fourier analysis for the Philippines tsunami showed that the governing periods of this tsunami are around 12 and 29 min (Table 6). The wavelet plot of the Ishigakijima record (Fig. 4b) shows that the first tsunami wave arriving in this station is dominated by the 11-min signal, followed by the 25-min signal. For this case, the periods of 11 and 25 min can be possibly attributed to the width and length of the seafloor rupture, respectively (Fig. 8). In Chichijima (Fig. 4c), located almost normal to the fault strike, the 15-min signal is the first one to arrive at this station and is dominating for almost the entire tsunami lifetime. This 15-min signal seems to be dictated by the width of the tsunami source. We note that we do not necessarily expect exactly the same signal resulting from source width at different stations. Taking into account the complex wave field generated by a tsunami due to irregular bathymetry, as well as tsunami source heterogeneity, the two signals of 11 and 15 min can be considered close enough to each other as both originated from the source width. In Naha, located at an angle of around 45 degrees relative to the source strike, the first and the dominating signal is the one at the period of 28 min, which seems to be dictated by the length of the tsunami source. For the two middle-class stations of Naha and Ishigakijima, i.e. neither located pure normal relative to the source strike nor pure lateral, it can be seen that in one of them the first signal is at 11 min and in the other it is at 28 min. In Wake Island, located truly

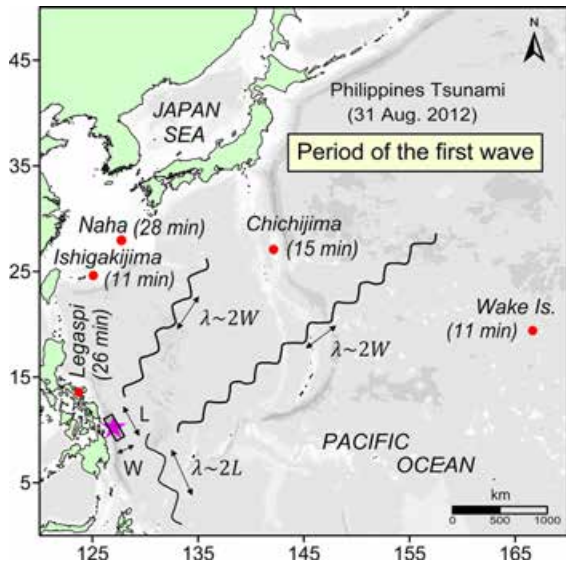


Figure 8

Sketch showing an approximation of the source location of the Philippines tsunami of 31 August 2012 (rectangle), and the first tsunami signals traveling towards the tide gauges located normal (e.g., Chichijima and Wake Island) and parallel (e.g., Legaspi) to the strike of the tsunami source. W and L represent width and length of the tsunami source, respectively. λ is the tsunami wavelength. Solid circles show the locations of the tide gauges

normal to the fault strike, the only tsunami signal is the 11-min signal, meaning that the spectra of the Wake Island station is mostly influenced by the width of the tsunami source rupture. For the Legaspi station, a pure lateral one, a first 26-min tsunami signal was recorded (Fig. 4b).

6.2. Tsunami Hazards for Southern Japan from Philippines Tsunamis

Analysis of sea level records of the 31 August 2012 Philippines tsunami revealed that the largest wave heights of this tsunami were recorded on tide gauges along the southern coast of Japan. Using numerical modeling of tsunami, it was shown above that a part of the waves generated by the Philippines tsunami was funneled towards southern Japan due to the bathymetric features in the Philippine Sea. According to LANDER *et al.* (2003), a similar observation was reported following the 3 May 1998 tsunami in the Philippine Sea (M_w 7.5), which was recorded in some Japanese

coastal sites such as Naha and Ishigakijima. Based on these observations, a large subduction earthquake offshore the Philippines is likely to generate damage along the southern coast of Japan, and hence, possible tsunami hazards for southern Japan from submarine earthquakes offshore the Philippines need to be considered.

7. Conclusions

The El Salvador tsunami of 27 August 2012 and the Philippines tsunami of 31 August 2012 were studied using 25 sea level records of these tsunamis and numerical modeling of tsunami waves. The main findings are as follows:

1. Among the analyzed sea level records for the El Salvador tsunami, the largest wave height was observed in Baltra (71.1 cm) at a distance of about 1,400 km from the tsunami source. Near-field stations of La Union and Acajutla recorded wave heights of 4.5 and 12.5 cm, respectively. Numerical modeling showed that most of the tsunami energy is directed towards the Galapagos Islands (including the Baltra sea level station), and possibly this is the reason for observing the maximum wave height of this tsunami in Baltra. Fourier and wavelet analyses revealed that the main tsunami peak periods are around 9 and 19 min for this tsunami, and the 45-min peak observed at some stations does not represent the tsunami source. The 9-min signal seems to be the main tsunami signal, as it was observed in many sea level spectra.
2. For the Philippines tsunami, the maximum wave height was observed at the Kushimoto station (30.5 cm), a Japanese tide gauge station located 2,700 km away from the source. Legaspi tide gauge station located in the near-field recorded a wave height of 4.2 cm. Relatively large wave heights were observed at tide gauges located along the coast of Japan. Numerical modeling showed that tsunami waves were funneled towards the southern coast of Japan. Numerical modeling also revealed that most of the Philippines tsunami energy was confined within the Philippine Sea

region. The main tsunami peak periods were estimated at around 8, 12 and 29 min. The strongest signal was at the period of around 12 min, as it was more common on the examined sea level spectra.

3. A connection was made between tsunami governing periods and source dimensions using wavelet analysis. Results may suggest that the dominant period of the first wave at stations normal to the fault strike usually reflects the fault width, while the period of the first wave at stations in the direction of fault strike most probably reflects the fault length.

Acknowledgments

The sea level data used in this study were provided through the USA National Oceanographic and Atmospheric Administration (NOAA), and UNESCO Intergovernmental Oceanographic Commission (IOC). We express our sincere gratitude to our colleagues from the sea level data centers at both NOAA and IOC for their invaluable efforts regarding the preparation, processing and timely supply of sea level data which has greatly contributed to tsunami science in the last decade. Figure 1 was drafted using the GMT software (WESSEL and SMITH 1991). The wavelet package by TORRENCE and COMPO (1998) was used in this study. This article benefitted from detailed and constructive reviews from two anonymous reviewers, for which we are sincerely grateful. We would like to thank Dr. Hermann Fritz (Georgia Institute of Technology, USA), the guest editor of this issue, for his assistance during the revision process of this article. This study was supported by the Alexander von Humboldt Foundation in Germany and the Japan Society for Promotion of Science (JSPS) in Japan.

REFERENCES

- BELL, C., VASSIE, J.M., and WOODWORTH, P.L. (2000). *POL/PSMSL Tidal Analysis Software Kit 2000 (TASK-2000), Permanent Service for Mean Sea Level*. CCMS Proudman Oceanographic Laboratory, UK, 22p.
- BEN-MENAHEM, A., and ROSENMAN, M. (1972). *Amplitude patterns of tsunami waves from submarine earthquakes*, J. Geophys. Res., 77, 3097–3128.
- BORRERO, J.C. and GREER, S.D. (2013). *Comparison of the 2010 Chile and 2010 Japan tsunamis in the Far-field*. Pure App. Geophys., 170(6–8):1249–1274.
- BORRERO, J. KALLIGERIS, N., LYNETT, P., FRITZ, H., NEWMANN, A. and CONVERS, J. (2014). *Observations and Modelling of the August 27, 2012 Earthquake and Tsunami affecting El Salvador and Nicaragua*. Pure App. Geophys., (in review).
- CNN (2012a). CNN news Agency, available at: <http://www.cnn.com/2012/08/27/world/americas/el-salvador-earthquake/index.html>. Accessed on 20 December 2012.
- CNN (2012b). CNN news Agency, available at: <http://www.cnn.com/2012/08/31/world/asia/philippines-earthquake/index.html>. Accessed on 20 December 2012.
- GLOBAL CMT (2012). *The Global Centroid-Moment-Tensor (CMT) Project*, available at: <http://www.globalcmt.org/>.
- HEIDARZADEH, M., and SATAKE, K. (2013a). *The 21 May 2003 Tsunami in the Western Mediterranean Sea: Statistical and Wavelet Analyses*. Pure App. Geophys., 170(9–10):1449–1462.
- HEIDARZADEH, M., and SATAKE, K. (2013b). *Waveform and Spectral Analyses of the 2011 Japan Tsunami Records on Tide Gauge and DART Stations Across the Pacific Ocean*. Pure App. Geophys., 170(6–8):1275–1293.
- IOC (Intergovernmental Oceanographic Commission), 2012, Sea Level Station Monitoring Facility, available at: <http://www.ioc-sealevelmonitoring.org/map.php>. Accessed on 20 December 2012.
- IOC, IHO, BODC (2003). Centenary edition of the GEBCO digital atlas, published on CD-ROM on behalf of the Intergovernmental Oceanographic Commission and the International Hydrographic Organization as part of the general bathymetric chart of the oceans. British oceanographic data centre, Liverpool.
- KANAMORI, H., and KIKUCHI, M. (1993). *The 1992 Nicaragua earthquake: a slow tsunami earthquake associated with subducted sediments*. Nature 361(6414):714–716.
- LANDER, J.F., WHITESIDE, L.S., LOCKRIDGE, P.A. (2003). *Two decades of global tsunamis 1982–2002*, Sci. Tsunami Hazards, 21(1), 3–88.
- MATHWORKS (2012). MATLAB user manual, The Math Works Inc., MA, USA, 282 p.
- NOAA (National Oceanographic and Atmospheric Administration), 2012, Center for Operational Oceanographic Products and Services (CO-OPS), National Ocean Service (NOS), at: <http://tidesandcurrents.noaa.gov/tsunami/>. Accessed on 22 December 2012.
- OKADA Y. (1985). *Surface deformation due to shear and tensile faults in a half-space*, Bull. Seismol. Soc. Am., 75(4), 1135–1154.
- PTWC (2012a), Pacific Tsunami Warning System- NOAA's National Weather Service, available at: <http://ptwc.weather.gov/ptwc/text.php?id=pacific.TIBPAC.2012.08.27.0445>. Accessed on 18 December 2012.
- PTWC (2012b), Pacific Tsunami Warning System- NOAA's National Weather Service, available at: <http://ptwc.weather.gov/text.php?id=pacific.TSUPAC.2012.08.27.0458>. Accessed on 18 December 2012.
- PTWC (2012c), Pacific Tsunami Warning System- NOAA's National Weather Service, available at: <http://ptwc.weather.gov/text.php?id=pacific.TSUPAC.2012.08.27.0627>. Accessed on 18 December 2012.

- PTWC (2012d), Pacific Tsunami Warning System- NOAA's National Weather Service, available at: <http://ptwc.weather.gov/text.php?id=pacific.TSUPAC.2012.08.31.1255>. Accessed on 18 December 2012.
- PTWC (2012e), Pacific Tsunami Warning System- NOAA's National Weather Service, available at: <http://ptwc.weather.gov/text.php?id=pacific.TSUPAC.2012.08.31.1454>. Accessed on 18 December 2012.
- RABINOVICH, A.B. (1997). *Spectral analysis of tsunami waves: Separation of source and topography effects*, J. Geophys. Res., 102 (12), 663–676.
- RABINOVICH, A.B., and THOMSON, R.E. (2007). *The 26 December 2004 Sumatra Tsunami: Analysis of Tide Gauge Data from the World Ocean Part 1. Indian Ocean and South Africa*, Pure App. Geophys., 164, 261–308.
- REUTERS (2012a). Reuters News Agency, available at: <http://www.reuters.com/article/2012/08/27/us-elsalvador-quake-idUSBRE87Q06E20120827>. Accessed on 18 December 2012.
- REUTERS (2012b). Reuters News Agency, available at: <http://www.reuters.com/article/2012/08/31/us-quake-philippines-idUSBRE87U0L720120831>. Accessed on 18 December 2012.
- SATAKE, K. (1988). *Effects of bathymetry on tsunami propagation: application of ray tracing to tsunamis*, Pure App. Geophys., 126(1):27–36.
- SATAKE, K., NISHIMURA, Y., PUTRA, P. S., GUSMAN, A. R., SUNENDAR, H., FUJII, Y., TANIOKA, Y., LATIEF, H. and YULIANTO, E. (2013). *Tsunami source of the 2010 Mentawai, Indonesia earthquake inferred from tsunami field survey and waveform modeling*, Pure App. Geophys., 170(9–10):1567–1582.
- TORRENCE, C., and COMPO, G. (1998), *A Practical Guide to Wavelet Analysis*, Bull. Am. Met. Soc., 79: 61–78.
- USGS (2012a). US Geological Survey—Global earthquake search, available at: <http://earthquake.usgs.gov/earthquakes/eqinthenews/2012/usc000c7yw/>. Accessed on 18 December 2012.
- USGS (2012b). US Geological Survey - Global earthquake search, available at: <http://earthquake.usgs.gov/earthquakes/eqinthenews/2012/usc000cc5m/>. Accessed on 18 December 2012.
- WELCH, P. (1967). *The use of fast Fourier transform for the estimation of power spectra: A method based on time averaging over short, modified periodograms*, IEEE Trans. Audio Electroacoust AE-15:70–73.
- WESSEL, P. and SMITH, W. H. F. (1991). *Free software helps map and display data*, EOS Trans. AGU 72:441.
- YALCINER, A.C., PELINOVSKY, E., TALIPOVA, T., KURKIN, A., KOZELKOV, A., ZAITSEV, A. (2004). *Tsunamis in the Black Sea: comparison of the historical, instrumental, and numerical data*. J. Geophys. Res., 109, C12023.

(Received February 25, 2013, revised January 10, 2014, accepted February 3, 2014)